Supplementary: Multi-color Holograms Improve Brightness in Holographic Displays

KORAY KAVAKLI, Koç University, Türkiye
LIANG SHI*, Massachusetts Institute of Technology, U.S.A.
HAKAN UREY, Koç University, Türkiye
WOJCIECH MATUSIK, Massachusetts Institute of Technology, U.S.A.
KAAN AKŞIT*, University College London, United Kingdom

ACM Reference Format:
Koray Kavaklı, Liang Shi, Hakan Urey, Wojciech Matusik, and Kaan Akşit. 2023. Supplementary: Multi-color Holograms Improve Brightness in Holographic Displays. In . ACM, New York, NY, USA, 25 pages. https://doi.org/10.1145/3610548.3618135

1 HOLOGRAPHIC DISPLAY HARDWARE

Our holographic display helps us to assess the image quality in our multi-color holograms and is also helpful for comparisons against conventional holograms. Figure 1 provides a photograph of our holographic display prototype.

Here, we provide a list of components used in our holographic display. It starts with a fiber-coupled multi-wavelength laser light source, LASOS MCS4, which combines three laser light sources peeking at 473 nm, 515 nm, and 639 nm. Two ESP32 boards control our multi-wavelength laser light source LASOS MCS-4. For accurate power control, we relied on Digital-to-Analog Converters (DAC) that are available on ESP32 boards. There is a pinhole aperture, Thorlabs SM1D12, after some distance concerning the fiber tip. This aperture helps us limit the diverging beams from our fiber. After this pinhole aperture, there is a linear polarizer, Thorlabs LPVISE100-A, which enables a polarization state aligned with our phase-only Spatial Light Modulator's fast axis (SLM) for light beams. Linearly polarized light beams reach our phase-only SLM, Holoeye Pluto-VIS, and get modulated with the optimized phase pattern. The phase-modulated beam arrives at a 4f imaging system composed of two 50 mm focal length achromatic doublet lenses, Thorlabs AC254-050-A, and a pinhole aperture, Thorlabs SM1D12, removing unmodulated and undiffracted light. In our experiments, we used a Ximea MC245CG-SY camera to capture the image reconstructions. We place our camera on an X-stage (Thorlabs PT1/M travel range: 0-25 mm, precision: 0.01 mm) and move it back and forth to capture photographs from various depth levels.

Discussion on the Off-Axis Holographic Display Prototype. The hardware prototype we employed for our experiments exhibits an off-axis configuration, wherein the direction of the diffracted beam is wavelength-dependent, resulting in chromatic aberrations as images move away from the Spatial Light Modulator (SLM) plane. These effects are evident in our 3D results, as depicted in Figure 9 of our manuscript. Specifically, both the front and back planes positioned 5 mm away from the SLM

*denotes corresponding authors

SA Conference Papers '23, December 12–15, 2023, Sydney, NSW, Australia

ACM ISBN 979-8-4007-0315-7/23/12.
https://doi.org/10.1145/3610548.3618135

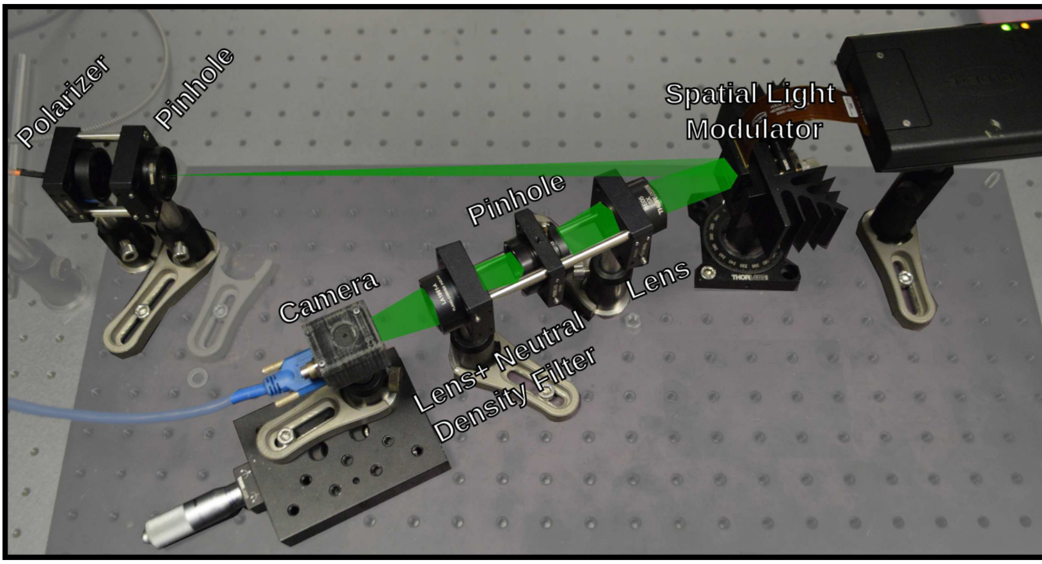

Fig. 1. A photograph showing our holographic display prototype used in assessing our multi-color holograms.

plane are susceptible to this issue. In contrast, on-axis configured holographic display prototypes hold the potential to overcome these aberrations by forming images on the zeroth diffraction order. However, it is crucial to note that on-axis systems inherently suffer from low contrast and limited dynamic range due to the presence of unmodulated beams. For off-axis holographic systems, there exist several avenues to mitigate the impact of chromatic aberrations:

Blazed Gratings. In theory, using blazed grating terms instead of linear phase gratings presents a viable solution to address the chromatic aberrations in off-axis systems. By incorporating blazed gratings, the misalignment of diffracted beams can be mitigated. However, a significant challenge lies in the practical implementation, as it necessitates sampling at a subpixel level of the SLM for each wavelength. Consequently, directly applying wavelength-dependent blazed gratings to rectify the misalignment of diffracted beams in holographic displays proves to be complex.

Improved Illumination Optics. An alternative approach involves precision optical design of the illumination optics. One potential method to rectify the misalignment of diffracted beams in off-axis holographic displays entails utilizing a spatially decentralized laser source with varying wavelengths, slightly tilted concerning their half-order diffraction angle. This solution requires three single-mode fibers, each carrying a distinct wavelength source. An alternative to avoid using three separate beams coupled to individual laser diodes involves employing specially designed optical hardware with prisms and RGB color filters. This setup efficiently filters and refracts the illuminated white light source into three primary colors, each following different paths [11] at the expense of light efficiency. Both of these methods hold promise in reducing chromatic aberrations and facilitating the overlapping of modulated hologram beams in the Fourier aperture plane.

2 EXTENDED LASER LOSS

In the main body of our manuscript, the laser loss of our method is described as

$$L_{\text{laser}} = \sum_{p=1}^{3}\left(\left(\sum_{t=1}^{T} l^2_{(p,t)}\right) - \max(I_p)s\right)^2. \tag{1}$$

This laser loss described in Eq. (1) could be further extended as L'_{laser} to avoid laser powers converging to zero or distributing unevenly. Our extension to Eq. (1) is as follows,

$$\begin{aligned} L'_{\text{laser}} = L_{\text{laser}} &+ \cos\left(\min\left(\sum_{p=1}^{3} l^2_{(p,t)}\right)\right) \\ &+ \cos\left(\min\left(\sum_{t=1}^{T} l^2_{(p,t)}\right)\right) \\ &+\left((Ts) - \sum_{p=1}^{3}\sum_{t=1}^{T} l^2_{(p,t)}\right)^2, \end{aligned} \tag{2}$$

In this extension, the first component we have to observe is as follows:

$$\cos\left(\min\left(\sum_{p=1}^{3} l^2_{(p,t)}\right)\right) \tag{3}$$

which helps to regularize the minimum value in the sum of laser powers across color primaries. This way, we ensure that the minimum total power for each color primary is non-zero. The second component,

$$\cos\left(\min\left(\sum_{t=1}^{T} l^2_{(p,t)}\right)\right), \tag{4}$$

help ensure that the total power for each frame is non-zero. These two components avoid hitting zero in terms of power for all frames and colors. The third and last component,

$$\left((Ts) - \sum_{p=1}^{3}\sum_{t=1}^{T} l^2_{(p,t)}\right)^2, \tag{5}$$

encourages the optimizer to meet the sum of laser power as large as the peak brightness level times the number of subframes. Thus, encouraging the optimized laser powers to meet the brightness demand for a given target.

3 OPTICAL BEAM PROPAGATION

Light transport models play a critical role in simulating coherent light used in holographic display applications (and more). We typically represent phase-only holograms used in a holographic display using a two-dimensional array filled with phase values ranging from $-\pi$ to π. We can also describe such a phase-only hologram in a complex notation, $O_h = e^{j\phi(x,y)}$, where ϕ represents the phase delay introduced by each pixel at a phase-only hologram. Holographic displays typically represent holograms, O_h, with programmable SLMs. A coherent beam U_i, again represented as a two-dimensional array, illuminates the phase-only hologram, O_h. Note that U_i is an oscillating electric field described as $U_i = A_0 e^{j(k\vec{r}+\phi_0(x,y))}$, where A_0 represents the amplitude of the optical beam, k, means the wavenumber that can be calculated as $\frac{2\pi}{\lambda}$, λ represents the wavelength of light, and ϕ_0 represents the initial phase of the optical beam. A_0 is often considered as $A_0 = 1$ for an ideal collimated beam, while ϕ_0 is assumed to be a two-dimensional array filled with random values between zero to 2π. Finally, leading to simplification of U_i as $e^{j\phi_0}$. In simple terms, as U_i illuminates O_h, U_i by modulated with O_h, forming a new modulated beam U_m that is calculated as

$$U_m = U_i O_h = e^{j(\phi(x,y)+\phi_0(x,y))}. \tag{6}$$

We form the reconstructed images at various depths as the modulated beam, U_m, propagates in free space away from the hologram plane (SLM plane). This propagation of optical beams from one plane to another follows the theory and method introduced by Rayleigh-Sommerfeld diffraction integrals [4]. This diffraction integral's first solution, the Huygens-Fresnel principle, is expressed as follows:

$$u(x,y) = \frac{1}{j\lambda} \int \int u_0(x,y) \frac{e^{jkr}}{r} \cos(\theta) dxdy, \tag{7}$$

Where the resultant field, $U(x,y)$, is calculated by integrating over every point across the hologram plane, $U_0(x,y)$ represents the optical field in the hologram plane for every point across XY plane (perpendicular to propagation direction), r represents the optical path between a selected point in hologram plane and a selected point in target plane, θ represents the angle between these points. The angular spectrum method, an approximation of the Huygens-Fresnel principle, is often simplified into a single convolution with a fixed spatially invariant complex kernel, $h(x,y)$ [16],

$$u(x,y) = u_0(x,y) * h(x,y) = \mathcal{F}^{-1}(\mathcal{F}(u_0(x,y))\mathcal{F}(h(x,y))). \tag{8}$$

In our implementations, we use a differentiable implementation of the light transport model found in Eq. (8), which we import from **GitHub:odak** [6, 9].

4 GRADIENT DESCENT OPTIMIZATION WITH DOUBLE PHASE CONSTRAINT

Our method aims to generate images that remain at the proximity of an SLM following the literature [12, 15]. Images in the proximity of an SLM are known for their high image quality. In this region, the light propagation distances r are typically a few millimeters. This region's most common phase-only hologram encoding method is the Double Phase (DP) [5] approach. DP method decomposes a complex field into a phase-only hologram. When optimizing holograms with Gradient Descent (GD) optimization, it is possible to introduce DP encoding into the optimization pipeline by defining a phase constraint [7]. Optimization can provide DP-encoded optimized holograms by constraining the phase updates of GD, ϕ of O_h. This constraint for ϕ can be written as a decomposition:

$$\begin{aligned}
\phi_0 &= \phi - \bar{\phi} \\
\phi_{\text{low}} &= \phi_0 - \text{offset} \\
\phi_{\text{high}} &= \phi_0 + \text{offset} \\
x_{\text{even}}, y_{\text{even}} &\in \{0, 2, 4, 6, \dots\} \\
x_{\text{odd}}, y_{\text{odd}} &\in \{1, 3, 5, 7, \dots\} \\
\phi[x_{\text{even}}, y_{\text{even}}] &= \phi_{\text{low}}[x_{\text{even}}, y_{\text{even}}] \\
\phi[x_{\text{odd}}, y_{\text{odd}}] &= \phi_{\text{low}}[x_{\text{odd}}, y_{\text{odd}}] \\
\phi[x_{\text{even}}, y_{\text{odd}}] &= \phi_{\text{high}}[x_{\text{even}}, y_{\text{odd}}] \\
\phi[x_{\text{odd}}, y_{\text{even}}] &= \phi_{\text{high}}[x_{\text{odd}}, y_{\text{even}}] \\
O_h &\leftarrow \phi,
\end{aligned} \tag{9}$$

, where offset is a variable to be optimized.

5 COMPARISON BETWEEN CONVENTIONAL AND MULTI-COLOR HOLOGRAM SCHEMES

This section compares additional results from conventional and multi-color schemes while targeting up to $\times 1.8$ peak intensity levels. Actual photographs of these comparisons are readily available in Fig. 2 and Fig. 3. In Fig. 4, we conducted a comparative analysis between multi-color holograms and conventional holograms with an higher laser power outputs. The evaluation of image quality indicates a significant drop in the case of conventional holograms with higher laser power output as the background noise increases in the images. Multi-color holograms also achieves similar or higher image quality with respect to conventional holograms at laser power outputs of $\times 1.5$ and $\times 2.0$, all while upholding the desired peak intensity levels. We also provide a pseudo-code for our conventional optimization routine, as in Listings 1. Readers can find our double-phase implementation structure in Sec. 4.

6 SIMULATED RESULTS

In Fig. 5, we provide full color simulated results along with the each individual reconstruction for each frame using our multi-color holograms when the target peak brightness is $\times 1.8$.

7 BEYOND $\times 1.8$ PEAK BRIGHTNESS LEVELS

Our method can also target peak brightness levels beyond $\times 1.8$ at the expense of color integrity. Beyond this threshold, our captures from our multi-color holograms resemble image artifacts similar to conventional holograms beyond $\times 1.0$. In Fig. 6, we provide additional captures acquired from our holographic display when the target peak intensity levels exceed $\times 1.8$ for multi-color hologram scheme.

8 MULTIPLANE MULTI-COLOR HOLOGRAMS

We provide additional three dimensional scene captures of the multiplane images that are generated with our multi-color hologram scheme in Fig. 7 and Fig. 8.

9 DYNAMIC INSENSITY SCALING

Our method's dynamic peak intensity scaling option allows increasing the peak brightness of the reconstructed images by simply setting a set of desired image qualities (image loss thresholds). We optimize the example experimental captures from our holographic display in Fig. 9 using a multi-color hologram dynamic intensity scale for various image qualities. From our experimental assessments in Fig. 9 and simulation-based assessments in Fig. 10, we conclude that aiming for lower image quality (higher image loss thresholds) enables a higher peak brightness at the expense of visual artifacts and color variations.

10 DIRECT PHASE REPRESENTATION

Our multi-color hologram scheme also supports direct phase encoding. We provide early image quality assessments showing slighly noisy results by switching to direct encoding from DP encoding. Direct phase results are presented in Fig. 11. We share these results to provide guidance for this important debate in the community regarding DP vs direct encoding.

11 SPATIAL COLOR SEPARATION AND CONTENT DEPENDENCY

We discuss at the manuscript of our paper that multi-color holograms could not benefit from brightness improvements and could have visual distortions when the target scene contains spatial

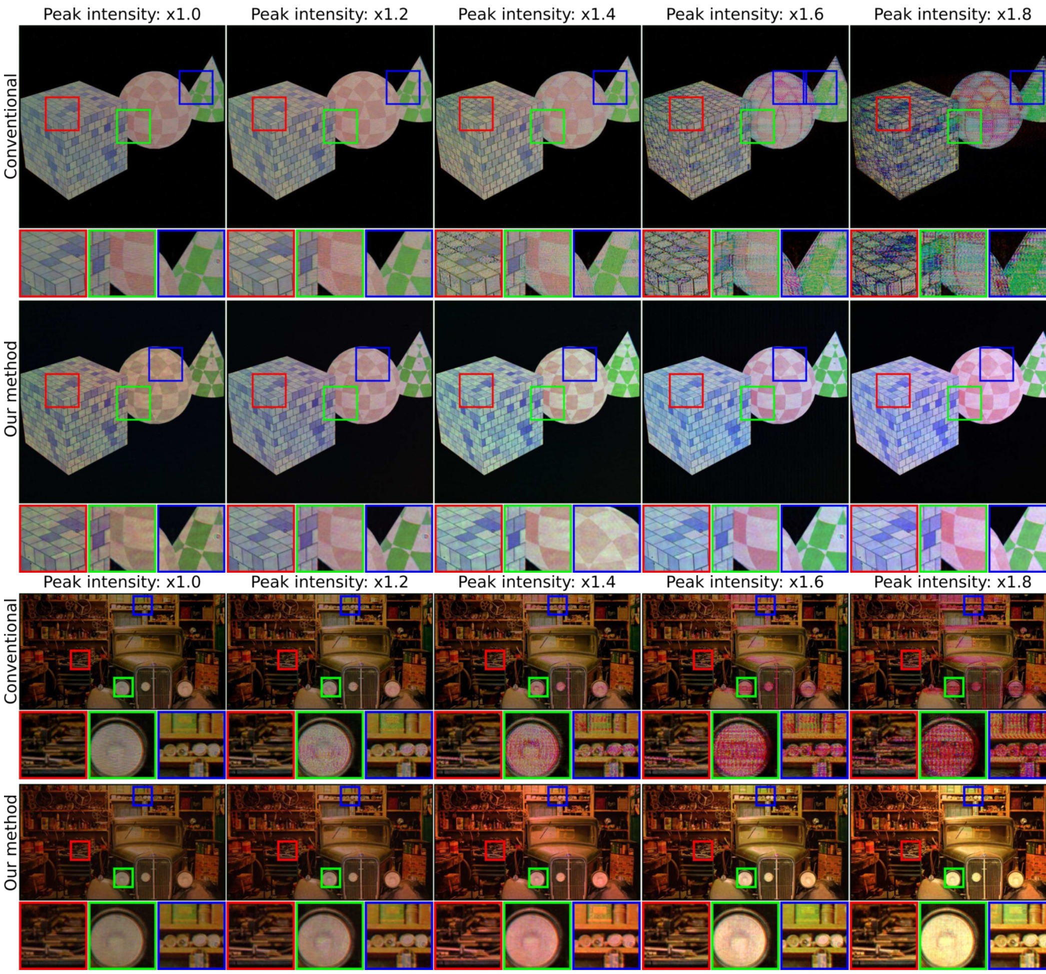

Fig. 2. Additional comparison between conventional and multi-color schemes. Photographs show that multi-color holograms can enhance the peak brightness levels of the captures up to ×1.8 without artifacts or distortions. All the images are generated on the Spatial Light Modulator (SLM) plane and captured with 140 ms exposure time using our holographic display. The conventional scheme fails to generate holograms that can target beyond ×1.0 brightness levels. (140 ms exposure).

color separation (e.g. each letter of a text is dedicated to one color primary). Although this is a very unlikely case in a display application, we provide a sample of the issue in Fig. 12.

12 REDUCING THE COST OF ILLUMINATION SOURCE

Our method can enable the use of low-power lasers in holographic displays and could provide a benefit on cost reduction for the development of holographic displays in the future. To illustrate this, let's consider two different laser diodes that are commercially available in Thorlabs: the HL6322G and the HL6312G. The HL6322G is a 15mW laser diode that costs \$77.45, while the HL6312G is a 5mW laser diode that costs \$24.45. The HL6322G is three times more expensive than the HL6312G.

Fig. 3. Increasing peak brightness levels with our multi-color holograms. Photographs show that our method can enhance the peak brightness levels of the captures up to ×1.8 without artifacts or distortions. In contrast, the conventional hologram fails to support beyond ×1.0 (140 ms exposure).

Fig. 4. Impact of increased laser power on conventional holograms. Photographs in the figure demonstrate the effect of elevated laser power on conventional holograms. Image quality assessment reveals a significant reduction in quality due to amplified background noise for conventional. Whereas, multi-color holograms achieve comparable image quality to conventional holograms at laser power outputs of ×1.5 and ×2.0 , while maintaining desired peak intensity levels. Notably, multi-color holograms exhibit better or same image quality metrics when targeting 1.5x intensity, while showing slight color balance deviations when targeting 2.0x peak intensities. (140 ms exposure time).

13 COLOR PERFORMANCE

Our method increases the brightness of holographic displays by utilizing its light sources more effectively through multi-color holograms. We find that the effectiveness of this brightness enhancement is content dependent. In other words, the degree of brightness enhancement could change depending on the target content. In some cases, going beyond what brightness level content allows could cause visual artifacts and a mismatch in color. To understand how, truthfully, our method could, in principle, maintain colors with varying brightness levels, we conduct a series of experiments in simulations. We chose a set of target images and optimized their multi-color holograms for varying brightness levels, ×1.0, ×1.2, ×1.4, ×1.6, and ×1.8. We compare simulated reconstructions of these optimized multi-color holograms with their corresponding targets at three separate depth levels, near, mid, and far, corresponding to 0 *mm*, 5 *mm*, and 10 *mm* away from SLM. Given the three color primaries used in our holographic display prototype, 473 *nm*, 515 *nm*, and 639 *nm*, we convert these reconstructions and their targets to trichromat sensations in the LMS cones of Human Visual System (HVS). We follow the exact conversion from RGB to LMS highlighted in the work by [3]. We calculate a Euclidean and Chamfer distance for each pair in LMS space to understand how close the simulated reconstructions are to their targets. The results of these comparisons in LMS space are provided in Fig. 13, Fig. 14, Fig. 15, and Fig. 16. We observe from

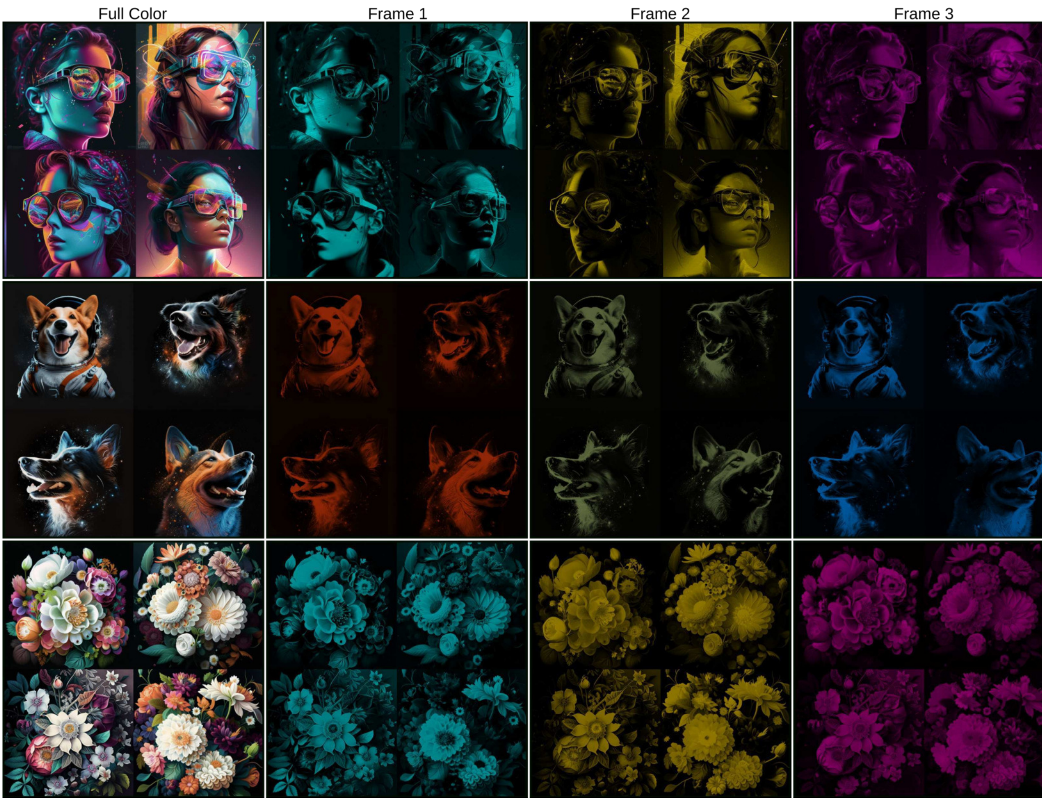

Fig. 5. Simulated results showing full color and each time frame reconstructions that are generated with our multi-color holograms when targetting ×1.8.

these assessments that our method mostly maintains color consistency with target scenes. However, higher brightness levels in some content could lead to perceptible color differences between target scenes and their corresponding solutions generated by our method (e.g. Fig. 16).

14 ITERATION COUNT

The number of iterations used in our method's optimization determines the final outcome's image quality and color performance. We compiled a figure as in Fig. 17 to demonstrate this relation. In this figure, we target Three-Dimensional (3D) scenes and rely on the exact configuration in our optimization code (e.g., defocus blur size in target images, propagation distances), where we choose a 1 cm volume 0.5 cm away from an SLM. Thus, we add a series of images in Fig. 17 to show how the solution increases iteration counts regarding defocus blur, color, and image quality. While fewer iterations could provide structurally correct images with incorrect colors, a larger number of iterations help generate color and improve image quality. The provided image quality metrics in Fig. 17 suggest that image quality increases with a larger iteration count, suggesting higher iteration count helps with the replication of features in target images (>500 iterations).

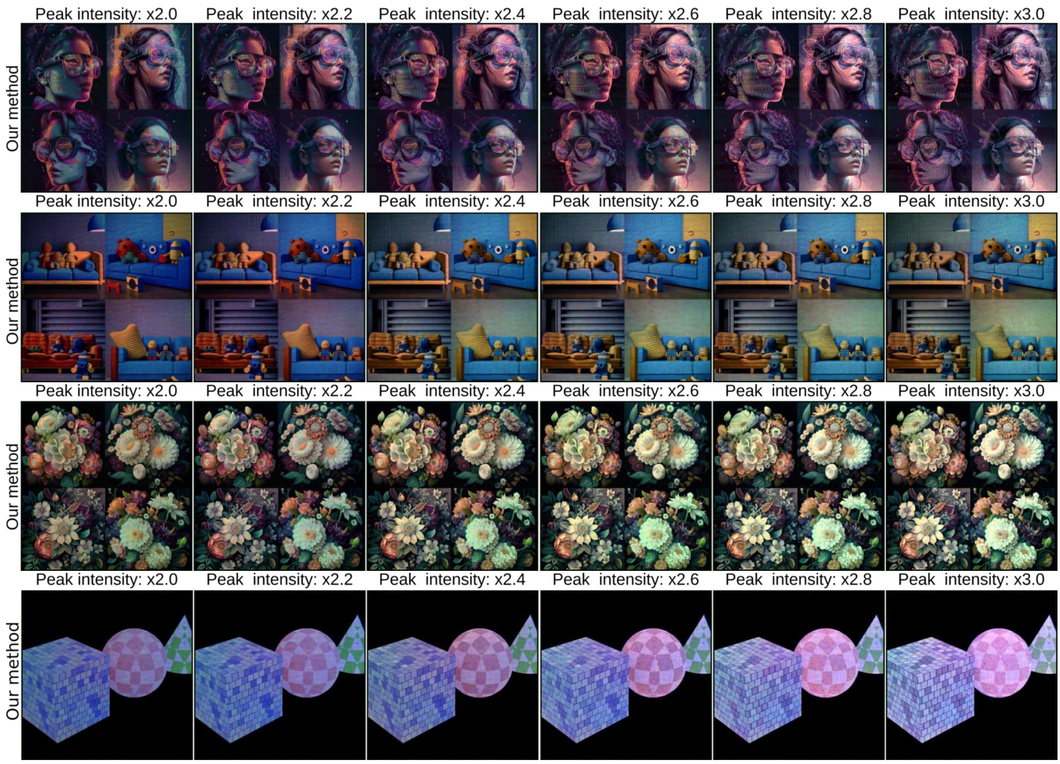

Fig. 6. Targeting beyond ×1.8 peak brightness levels. Photographs showing our multi-color holograms generating higher brightness beyond ×1.8 (50 ms exposure time)

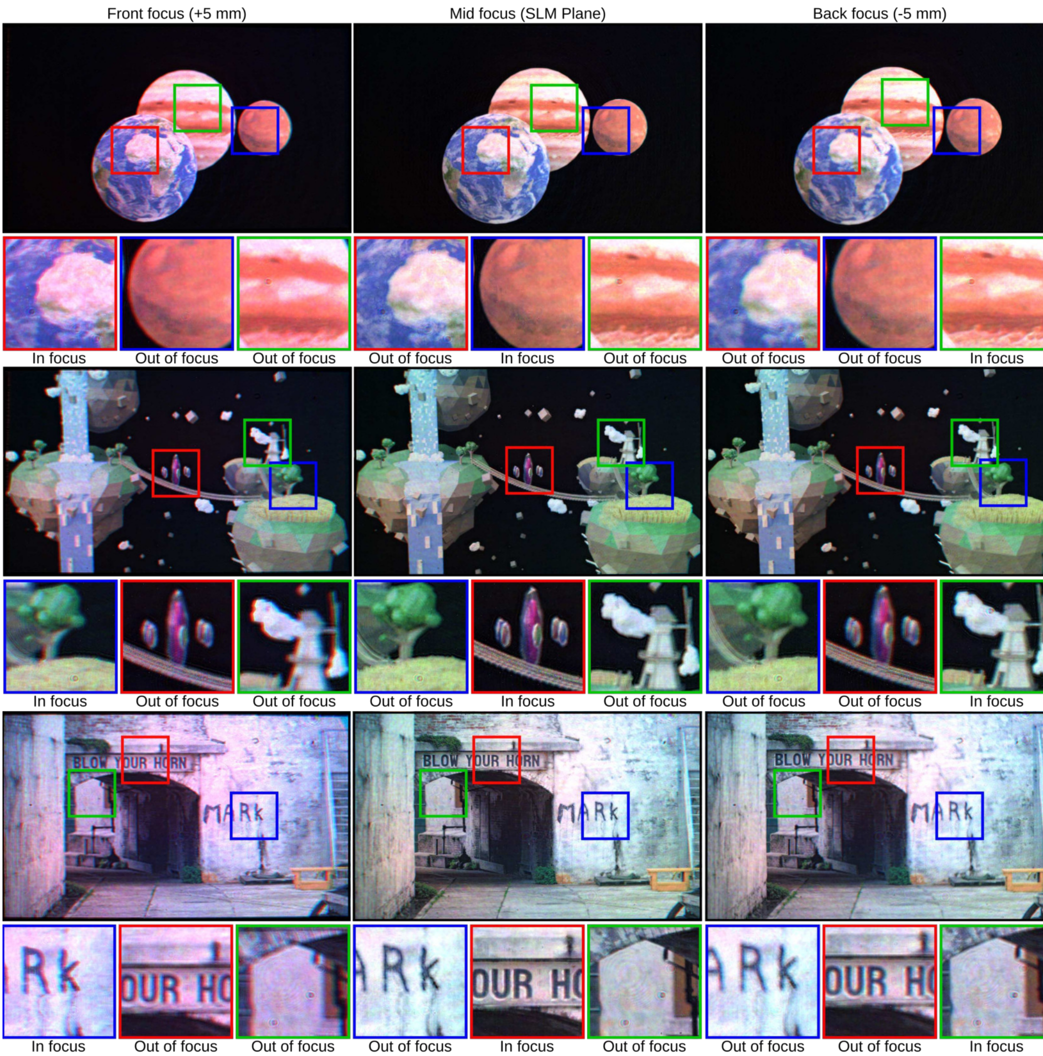

Fig. 7. Three dimensional scenes using our multi-color holograms. Photographs show a multiplane image generated by our multi-color hologram scheme with three focus planes. The targeted brightness level is ×1.8. (150 ms exposure time)

Fig. 8. Three dimensional scenes using our multi-color holograms. Photographs show a multiplane image generated by our multi-color hologram scheme with three focus planes. The targeted brightness level is ×1.8. (150 ms exposure time)

Fig. 9. Dynamic intensity scaling using our method. Photographs of the images that are generated with different image loss threshold by our multi-color hologram dynamic intensity scaling. The optimized peak intensity levels for the first row: ×1.61, ×1.87 and ×2.04 and the second row: ×1.61, ×1.27 and ×1.45 is ×2.23. (100 ms exposure time)

Fig. 10. Dynamic intensity scaling using our method. Simulated images that are generated with different image loss threshold by our multi-color hologram dynamic intensity scaling. The optimized peak intensity levels for the first row: ×1.46, ×2.17 and ×2.57, the second row: ×1.76, ×2.24 and ×2.47, and the third row: ×2.1, ×3.13 and ×3.36.

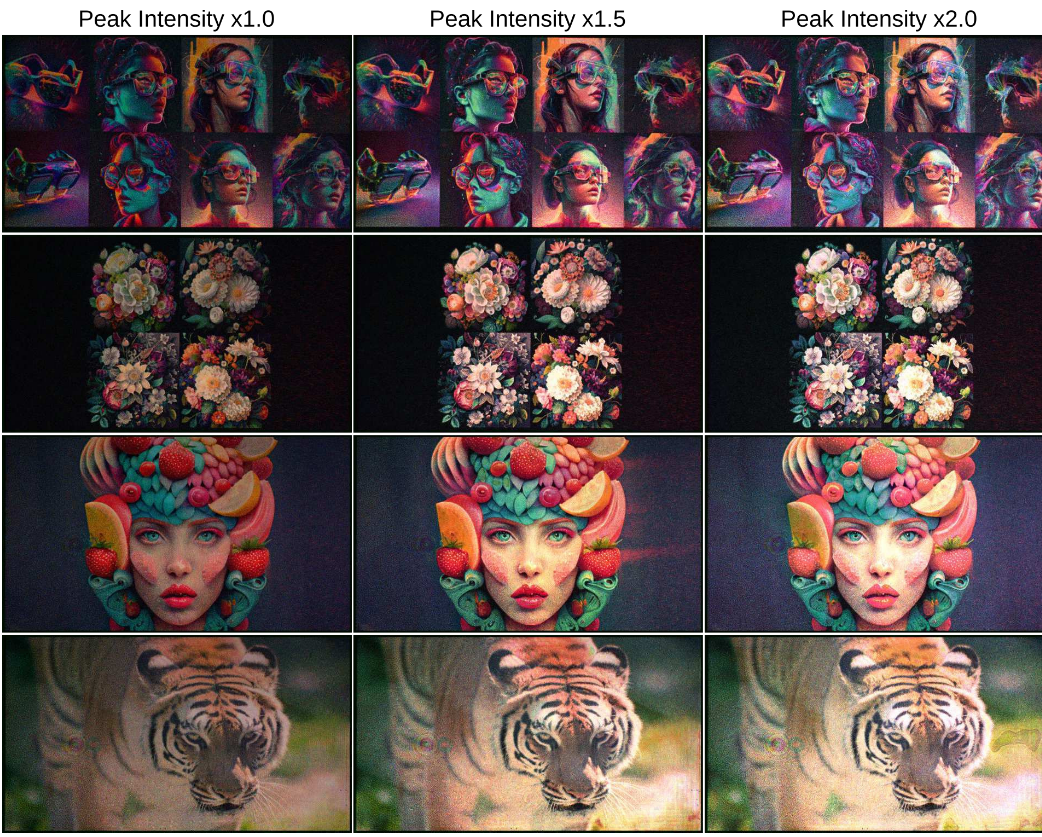

Fig. 11. Captured images for direct phase holograms at Spatial Light Modulator (SLM) plane. Photographs showing our multi-color holograms with direct phase encoding can support higher brightness levels. (140 ms exposure time).

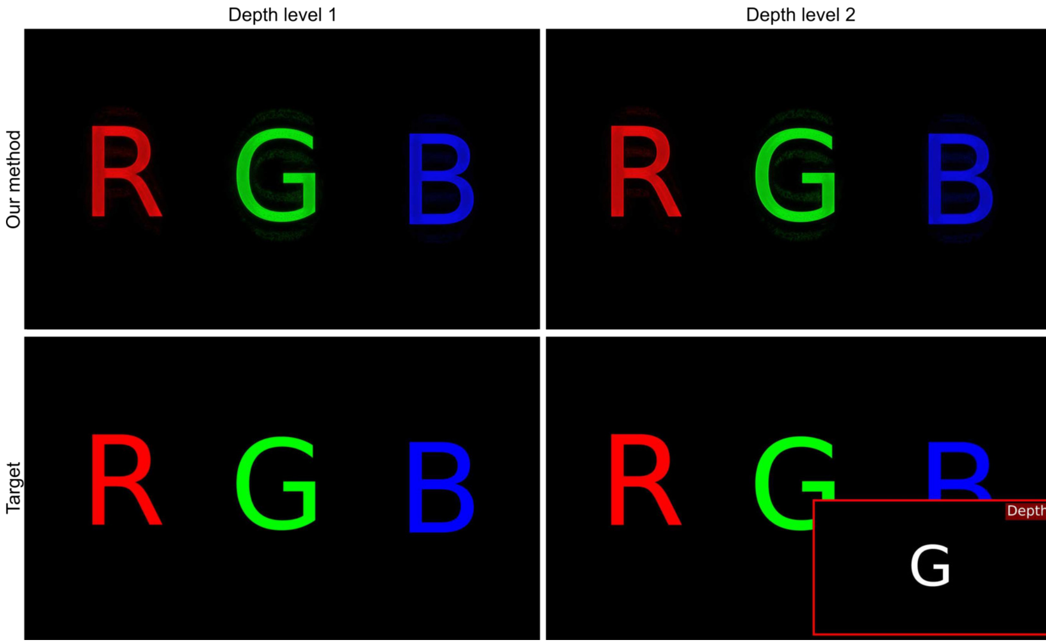

Fig. 12. Simulated reconstruction of our multi-color holograms when they target scenes with spatial color separation (e.g. each letter of a text is dedicated to one color primary) and ×1/8 brightness. Although a corner case, multi-color holograms could not benefit from brightness improvements in such cases while leading to visual distortions.

```
import torch.optim as optim
from odak import propagate_beam,generate_complex_field

# Provide an initial phase for a hologram (random, manual or learned).
$\phi_{f_n}$ = define_initial_phase(type='random')
$\phi_{f_n}$.requires_grad = True
# Provide number of iterations requested.
iter_no= 200
# Setup a solver with
optimizer = optim.Adam([{'params': $\phi_{f_n}$, $offset_{f_n}$}],lr=0.002)
# Calculate targets for each plane.
$P_0, P_1, P_2, ..., P_n$ = targetting_scheme(distances)

# Iterates until iteration number is met.
for i in range(iter_no):
    # Distances between a hologram and target image planes.
    for distance_id,distance in enumerate(distances):
        # Clearing gradients.
        optimizer.zero_grad()
        # Phase constrain (Equation 5).
        $\phi$ = phase_constrain($\phi$, $offset$)
        # Generates a hologram with the latest phase pattern.
        $O_h$ = generate_complex_field(1., $\phi$)
        # Forward model.
        $K$ = propagate($O_h$, distance)
        # Calculating loss function for the reconstruction.
        loss += $\mathcal{L}_m$($|U|^2$, $P_{(distance\_id)}$)
        # Updating the phase pattern using accumulated losses.
        loss.backward()
        optimizer.step()

# Optimized multiplane hologram:
$\phi \rightarrow O_h$
```

Listings 1: Stochastic-Gradient based multiplane phase-only hologram optimization algorithm when reconstructing images at a spatial light modulator plane. The abstraction is Pythonic. Note that this optimization runs for each color channel separately.

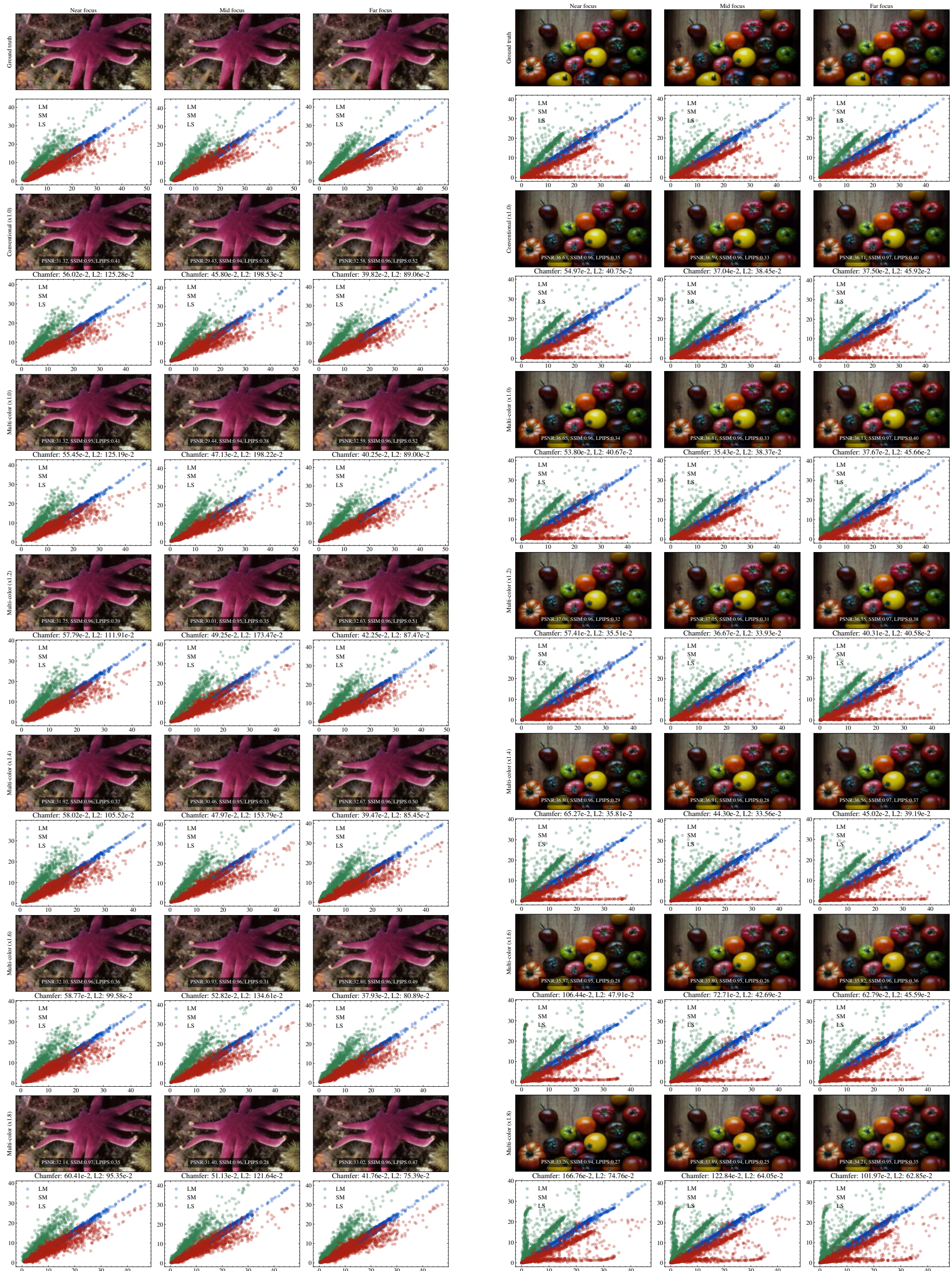

(a) (b)

Fig. 13. We evaluate our method's color performance for various target scenes in simulation. We provide a target reconstruction for each case and their perceived color levels in LMS space, precisely plotted LM, LS, and MS pairs (see for exact conversion from RGB to LMS [3]). We observe that our method truthfully generates colors for varying brightness levels in most cases. Sometimes, there could be a perceptible color mismatch when aiming for higher brightness levels (e.g. ×1.8 enhancement).

(a) (b)

Fig. 14. We evaluate our method's color performance for various target scenes in simulation. We provide a target reconstruction for each case and their perceived color levels in LMS space, precisely plotted LM, LS, and MS pairs (see for exact conversion from RGB to LMS [3]). We observe that our method truthfully generates colors for varying brightness levels in most cases. Sometimes, there could be a perceptible color mismatch when aiming for higher brightness levels (e.g. ×1.8 enhancement).

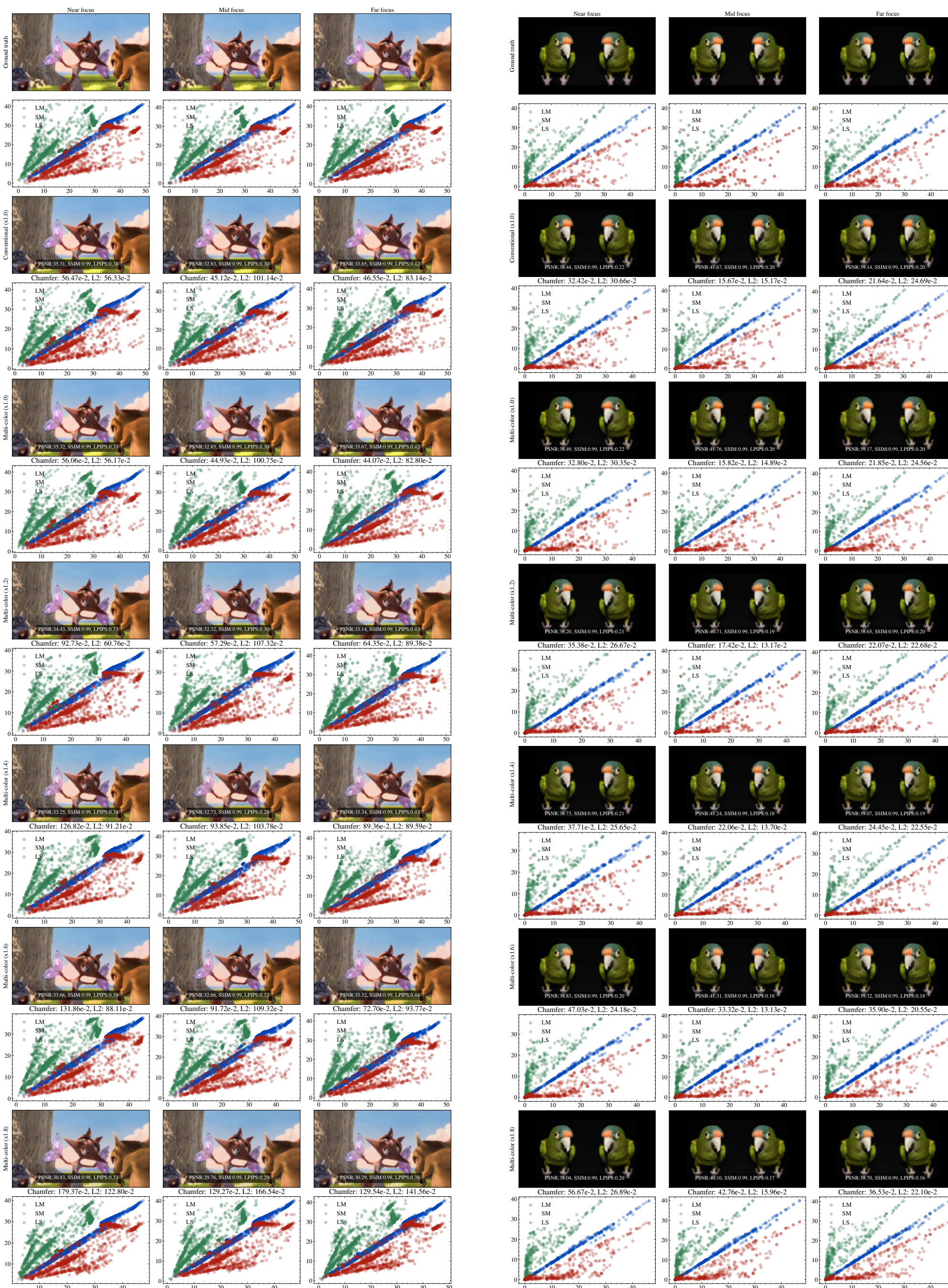

(a) (b)

Fig. 15. We evaluate our method's color performance for various target scenes in simulation. We provide a target reconstruction for each case and their perceived color levels in LMS space, precisely plotted LM, LS, and MS pairs (see for exact conversion from RGB to LMS [3]). We observe that our method truthfully generates colors for varying brightness levels in most cases. Sometimes, there could be a perceptible color mismatch when aiming for higher brightness levels (e.g. ×1.8 enhancement).

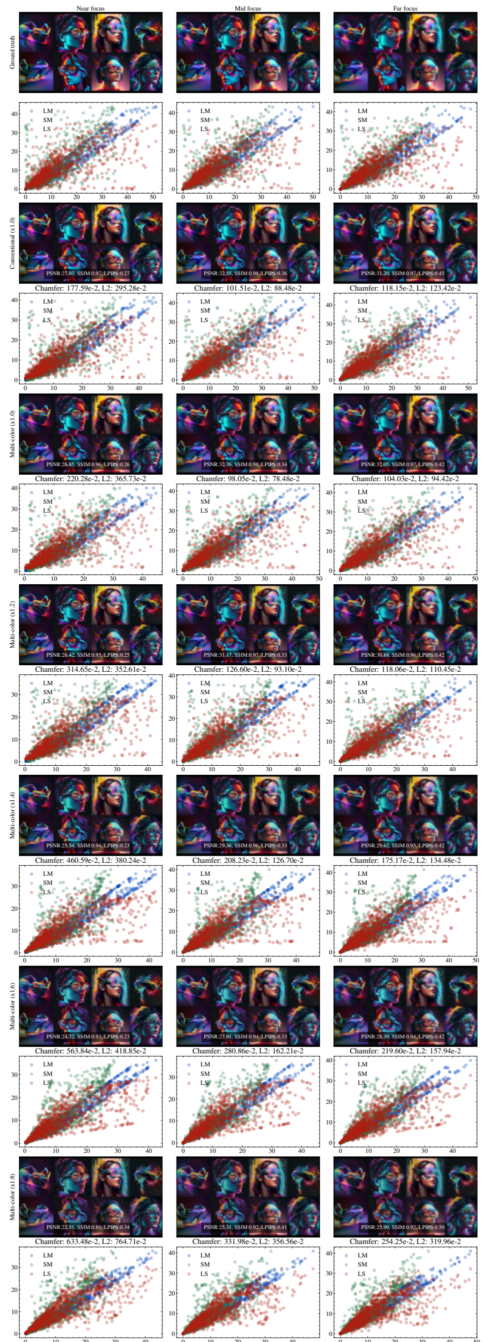

(a)

Fig. 16. We evaluate our method's color performance for various target scenes in simulation. We provide a target reconstruction for each case and their perceived color levels in LMS space, precisely plotted LM, LS, and MS pairs (see for exact conversion from RGB to LMS [3]). We observe that our method truthfully generates colors for varying brightness levels in most cases. Sometimes, there could be a perceptible color mismatch when aiming for higher brightness levels (e.g. ×1.8 enhancement).

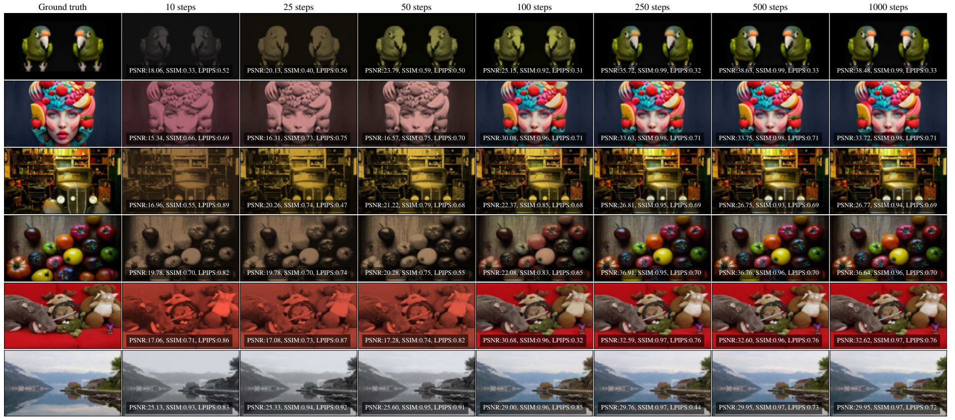

(a)

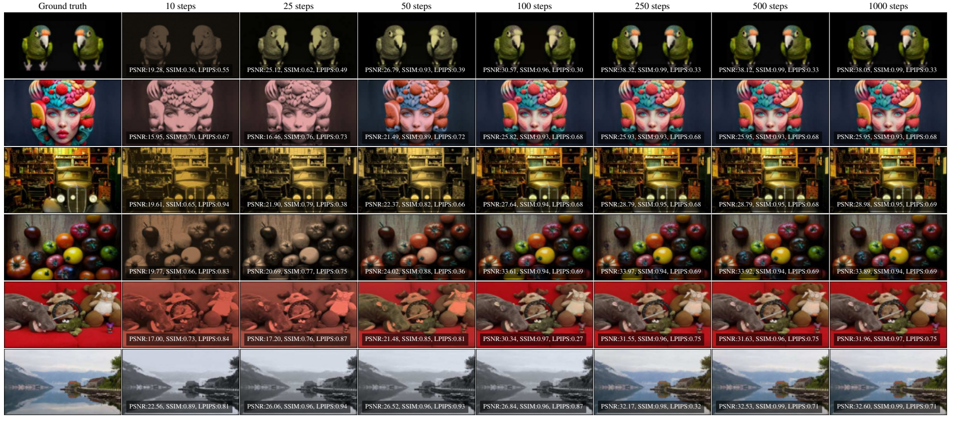

(b)

Fig. 17. We provide two sets of simulated reconstructions for solutions using various iteration count in our method's optimizations. These two sets of simulated reconstructions shows a single depth plane of three plane target scene. The set at the top is generated with a target brightness at ×1.0, while the bottom set is targeting ×1.8.

15 RESULTS FROM ON-AXIS HOLOGRAPHIC DISPLAY CONFIGURATION

Our methodology is also applicable to holographic display prototypes configured in an on-axis imaging setup. In order to illustrate the adaptability of our approach to on-axis holographic displays, we constructed an additional holographic display configured for on-axis operation.

For the on-axis configured holographic display prototype we decided to employ RGB LEDs as a substitute for lasers. Because of this substitution and the subsequent limited calibration possibilities, our results in this configuration remain as preliminary work. Therefore this section serves the purpose of demonstrating our method can support on-axis configurations. The results obtained from the on-axis configuration are absent from chromatic aberrations, a challange that is faced by off-axis holographic display prototypes. Both DP and direct phase encoded results are presented in Fig. 18 and Fig. 19.

Here, we provide a list of components used in our on-axis holographic display. It starts with a RGB LED light source, ws2812b (466 nm, 524 nm, 623 nm), that is controlled by an Arduino UNO board. A pinhole aperture, the Thorlabs SM1D12, is positioned infront of the RGB LED source to confine beam divergence. Following to this aperture, we employed a 4f optical setup, composed of the AC508-075-A-ML and AC254-035-A-ML components, thereby further reducing the spot size of our RGB LED light source. Another Thorlabs SM1D12 pinhole aperture follows this 4f system. Positioned after this second aperture is a collimator lens, the AC254-050-A-ML, accompanied by a linear polarizer, the Thorlabs LPVISE100-A. This polarizer is carefully aligned with the fast axis of our phase-only Spatial Light Modulator (SLM) to ensure precise beam alignment. The linearly polarized light beams then reach our phase-only SLM, Holoeye Pluto-VIS. The phase-modulated beam proceeds to a 4f imaging system, consisting of a 75 mm achromatic doublet lens (AC508-075-A-ML), a Thorlabs SM1D12 pinhole aperture, and a 35 mm achromatic doublet lens (AC254-035-A-ML). To capture the resultant image reconstructions, we employ the Ximea MC245CG-SY camera.

Fig. 18. Three dimensional scene captured with on-axis holographic display prototype using our multi-color DP encoded holograms. Photographs show a multiplane image generated by our multi-color DP coded hologram scheme with three focus planes. The front and back focus planes are remain 5 mm away from the SLM while the middle plane remains on the SLM plane. The targeted brightness level is ×1.8. (450 ms exposure time)

16 ADDITIONAL DISCUSSIONS

Eyebox. Producing a wide eyebox in holographic displays is critical for the success of holographic glasses for Augmented Reality (AR) and Virtual Reality (VR) applications. Recent studies explore eyebox qualities in holographic displays for various optimization methods [10] (e.g. GD

Fig. 19. Images captured with on-axis holographic display prototype using our multi-color direct phase encoded holograms. Photographs show images that are generated 30 mm in front of the SLM using our multi-color direct phase encoded hologram scheme. The targeted brightness levels for all scenes is $\times 1.8$. (450 ms exposure time)

or Gerchberg-Saxton). A similar study could help characterize eyebox qualities in our method. In addition, moving away from DP encoding towards direct encoding in our method may help co-optimizing image quality and eyebox size. Currently, our method supports both DP and direct-phase encoding. In our supplementary, we provide early image quality assessments showing noisier results by switching to direct encoding. Our study suggests that regularizing image loss per eyebox size could be necessary for the following works.

Hardware-in-the-loop. Our method can also benefit from hardware-in-the-loop techniques [2, 8, 13] to calibrate our holographic display. However, these methods require a dedicated new investigation to operatein multi-color hologram scheme. We leave these for future investigations.

Diffraction Efficiency. The fraction of the incident optical power appearing in a diffracted order, diffraction efficiency, is driven by the aperture shape, reflection, and transmission efficiency of an SLM [14]. Regardless of hardware, conventional and multi-color holograms are optimized using diffraction integral simulations. These simulations don't regularize their power distribution beyond the image area. Their hologram-related diffraction efficiency correlates strongly with the design choices of their hologram generation pipelines. We leave a thorough diffraction-efficiency comparison analysis of various pipelines in the literature as a future work.

REFERENCES

[1] Eirikur Agustsson and Radu Timofte. 2017. NTIRE 2017 Challenge on Single Image Super-Resolution: Dataset and Study. In *The IEEE Conference on Computer Vision and Pattern Recognition (CVPR) Workshops*.

[2] Praneeth Chakravarthula, Ethan Tseng, Tarun Srivastava, Henry Fuchs, and Felix Heide. 2020. Learned Hardware-in-the-Loop Phase Retrieval for Holographic near-Eye Displays. *ACM Trans. Graph.* 39, 6, Article 186 (nov 2020), 18 pages. https://doi.org/10.1145/3414685.3417846

[3] Ahmet H Güzel, Jeanne Beyazian, Praneeth Chakravarthula, and Kaan Akșit. 2023. ChromaCorrect: prescription correction in virtual reality headsets through perceptual guidance. *Biomedical Optics Express* 14, 5 (2023), 2166–2180.

[4] John C Heurtley. 1973. Scalar Rayleigh–Sommerfeld and Kirchhoff diffraction integrals: a comparison of exact evaluations for axial points. *JOSA* 63, 8 (1973), 1003–1008.

[5] C K Hsueh and A A Sawchuk. 1978. Computer-generated double-phase holograms. *Appl. Opt.* 17, 24 (Dec. 1978), 3874–3883.

[6] Koray Kavakli and Kaan Akşit. 2022. Introduction to Odak: a Differentiable Toolkit for Optical Sciences, Vision Sciences and Computer Graphics, In Frontiers in Optics + Laser Science 2022 (FIO, LS). *Frontiers in Optics + Laser Science 2022 (FIO, LS)*, FTu1A.1. https://doi.org/10.1364/FIO.2022.FTu1A.1

[7] Koray Kavaklı, Yuta Itoh, Hakan Urey, and Kaan Akşit. 2023. Realistic Defocus Blur for Multiplane Computer-Generated Holography. *IEEE VR 2023* (March 2023). https://doi.org/10.1109/VR55154.2023.00057

[8] Koray Kavaklı, Hakan Urey, and Kaan Akşit. 2022. Learned holographic light transport. *Applied Optics* 61, 5 (2022), B50–B55.

[9] Koray Kavakli, David Robert Walton, Nick Antipa, Rafał Mantiuk, Douglas Lanman, and Kaan Akşit. 2022. Optimizing vision and visuals: lectures on cameras, displays and perception. In *ACM SIGGRAPH 2022 Courses*. 1–66.

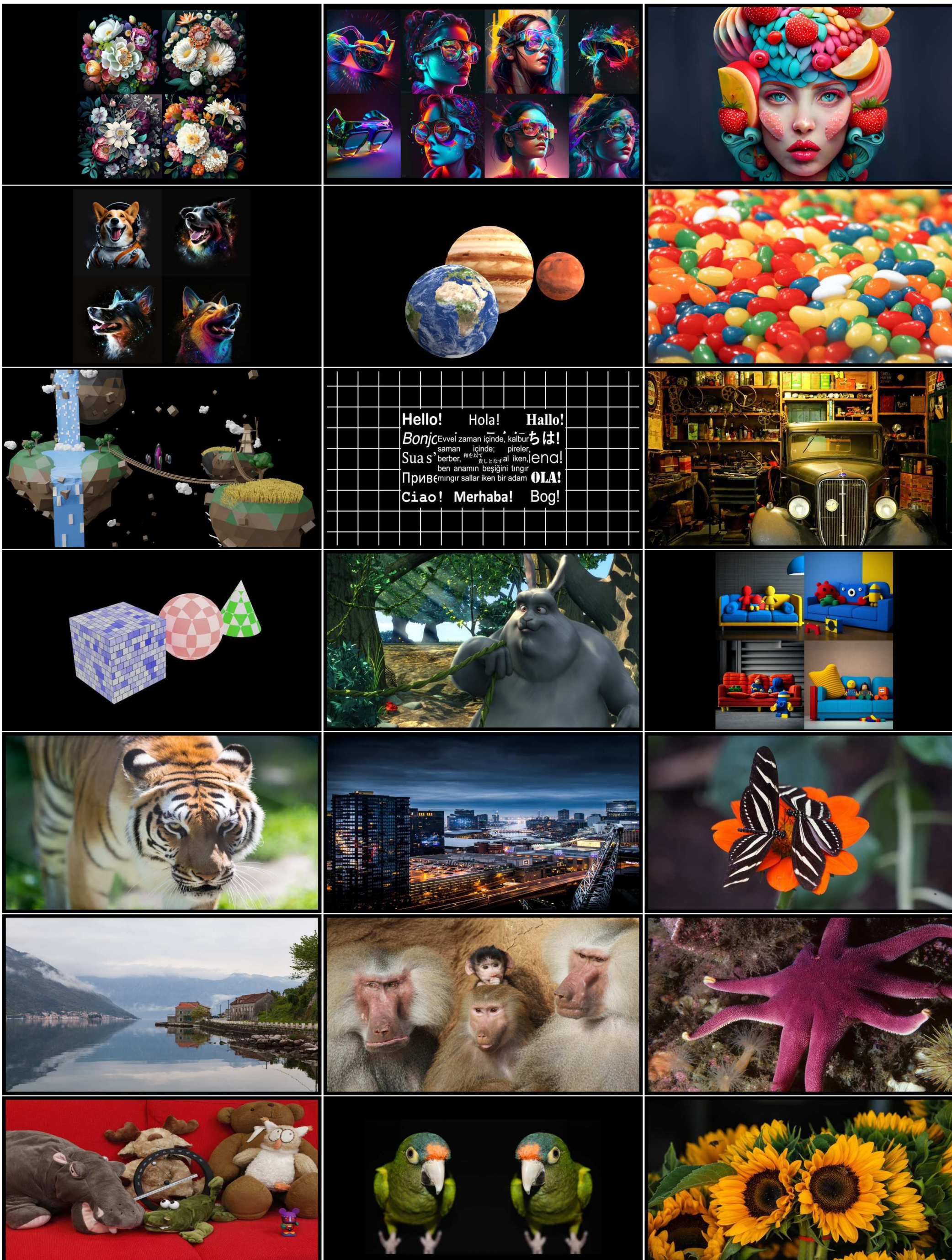

Fig. 20. A gallery of target images used in our manuscript and supplementary (Source link: **Github:complight/image**, DIV2K [1]).

[10] Dongyeon Kim, Seung-Woo Nam, Byounghyo Lee, Jong-Mo Seo, and Byoungho Lee. 2022. Accommodative holography: improving accommodation response for perceptually realistic holographic displays. *ACM Transactions on Graphics (TOG)* 41, 4 (2022), 1–15.

[11] Shu-Feng Lin, Di Wang, Qiong-Hua Wang, and Eun-Soo Kim. 2020. Full-color holographic 3D display system using off-axis color-multiplexed-hologram on single SLM. *Optics and Lasers in Engineering* 126 (2020), 105895. https://doi.org/10.1016/j.optlaseng.2019.105895

[12] Andrew Maimone, Andreas Georgiou, and Joel S Kollin. 2017. Holographic near-eye displays for virtual and augmented reality. *ACM Trans. Graph.* 36, 4 (July 2017), 1–16.

[13] Yifan Peng, Suyeon Choi, Nitish Padmanaban, and Gordon Wetzstein. 2020. Neural holography with camera-in-the-loop training. *ACM Transactions on Graphics (TOG)* 39, 6 (2020), 1–14.

[14] Krishnendu Samanta, Joby Joseph, Balpreet Singh Ahluwalia, and Krishna Agarwal. 2019. Study of electric fields of diffraction from spatial light modulator: discussion. *JOSA A* 36, 10 (2019), 1778–1786.

[15] Liang Shi, Beichen Li, Changil Kim, Petr Kellnhofer, and Wojciech Matusik. 2021. Towards real-time photorealistic 3D holography with deep neural networks. *Nature* 591, 7849 (2021), 234–239.

[16] Maciej Sypek. 1995. Light propagation in the Fresnel region. New numerical approach. *Optics communications* 116, 1-3 (1995), 43–48.